The Astro-E High Resolution X-Ray Spectrometer

Richard L. Kelley[a†], Michael D. Audley[c,e], Kevin R. Boyce[a], Susan R. Breon[a], Ryuichi Fujimoto[e], Keith C. Gendreau[b], Stephen S. Holt[a], Yoshitaka Ishisaki[f], Dan McCammon[d], Tatehiro Mihara[g], Kazuhisa Mitsuda[e], S. Harvey Moseley[a], D. Brent Mott[a], F. Scott Porter[a], Caroline K. Stahle[a], and Andrew E. Szymkowiak[a]

[a]NASA/Goddard Space Flight Center, USA
[b]Department of Astronomy, University of Maryland, USA
[c]Universities Space Research Association, USA
[d]Department of Physics, University of Wisconsin, USA
[e]Institute of Space and Astronautical Science (ISAS), Japan
[f]Tokyo Metropolitan University, Japan
[g]The Institute of Physical and Chemical Research (RIKEN), Japan

ABSTRACT

The Astro-E High Resolution X-ray Spectrometer (XRS) was developed jointly by the NASA/Goddard Space Flight Center and the Institute of Space and Astronautical Science in Japan. The instrument is based on a new approach to spectroscopy, the X-ray microcalorimeter. This device senses the energies of individual X-ray photons as heat with extreme precision. A 32 channel array of microcalorimeters is being employed, each with an energy resolution of about 12 eV at 6 keV (the Fe-K region). This will provide spectral resolving power 10 times higher than any other non-dispersive X-ray spectrometer. The instrument incorporates a three stage cooling system capable of operating the array at 60 mK for about two years in orbit. The array sits at the focus of a grazing incidence conical mirror. The quantum efficiency of the microcalorimeters and the reflectivity of the X-ray mirror system combine to give high throughput over the 0.3-12 keV energy band. This new capability will enable the study of a wide range of high-energy astrophysical sources with unprecedented spectral sensitivity. This paper presents the basic design requirements and implementation of the XRS, and also describes the instrument parameters and performance.

Keywords: detectors, calorimeters, bolometers, x-ray, spectrometer, instruments, missions

1. Introduction

Breakthroughs in astrophysics generally come from the development of powerful new instruments that bring enhanced capabilities to astrophysicists who are studying the weak signals from celestial objects. The high resolution X-Ray Spectrometer (XRS) on the Astro-E observatory was developed to substantially increase (by a factor of 10) the spectral resolving power and quantum efficiency for celestial spectroscopy in the 0.3-12 keV band. The Astro-E X-ray observatory will be the fifth in a series of highly successful X-ray observatories developed by the Institute of Space and Astronautical Science (ISAS) in Japan[1, 2], with significant contributions from the US. The basic features of Astro-E are high spectral resolution and broad band X-ray spectroscopy. Previously, high spectral resolution, defined here as several eV, required the use of wavelength dispersive devices such as gratings and crystals. While these devices are capable of the highest spectral resolution available, this comes at the cost of quantum efficiency and a limited capability for studying sources that are extended by more than about an arc-minute. The XRS will employ a new type of X-ray spectrometer, the single photon X-ray microcalorimeter, to obtain an energy resolution of ~ 12 eV (FWHM) over the 0.3-12 keV energy band. The primary purpose of the XRS is to provide high resolution X-ray spectroscopy, but it does have a limited ability to image over a 2' × 4' field of view. The true imaging capability on Astro-E will be provided by the X-ray Imaging Spectrometer (XIS), which has higher collecting area, a larger field-of-view (~ 18' × 18') and moderate spectral resolving power (~ 120 eV at 6 keV). The instrument consists of a set of four independent X-ray CCD cameras[3].

† Correspondence: email: Richard.L.Kelley.1@gsfc.nasa.gov

Both the XRS and the four CCD cameras of the XIS use the next generation of high throughput conical foil X-ray mirrors[4]. These mirrors use the basic nested, coated foil concept, but the reflective surface is replicated off a polished mandrel. The half power diameter will be about 2', or about half that of ASCA, and there will be much less scattered power beyond a few arc-minutes due to the better surfaces, resulting in a narrower core in the point-spread function. The four mirrors for the XIS cameras have a focal length of 4.75 meters, an outer diameter of 40 cm, and gold reflecting surfaces. The total effective area of the XIS will be some 4-6 times higher than that of the SIS instruments on the ASCA Observatory. The XRS mirror has a 4.5-meter focal length and platinum surfaces. Platinum was chosen because of its 10-15% higher reflectivity around 6 keV to increase the throughput of the XRS. The mirrors were developed at Goddard with help from teams at Nagoya University and ISAS.

The band pass of Astro-E will be extend all the way up to ~ 700 keV using the Hard X-ray Detector (HXD). This instrument was developed primarily at Tokyo University and ISAS[5]. It is based on collimated gadolinium silicate well-type phoswich counters and silicon PIN diodes to give a composite band pass of 10-700 keV. The HXD has low residual instrumental background, which results in significantly higher sensitivity than previous missions in the high energy band. Estimates are that the sensitivity will be up to 10 times higher than the HEXTE on the RXTE Observatory.

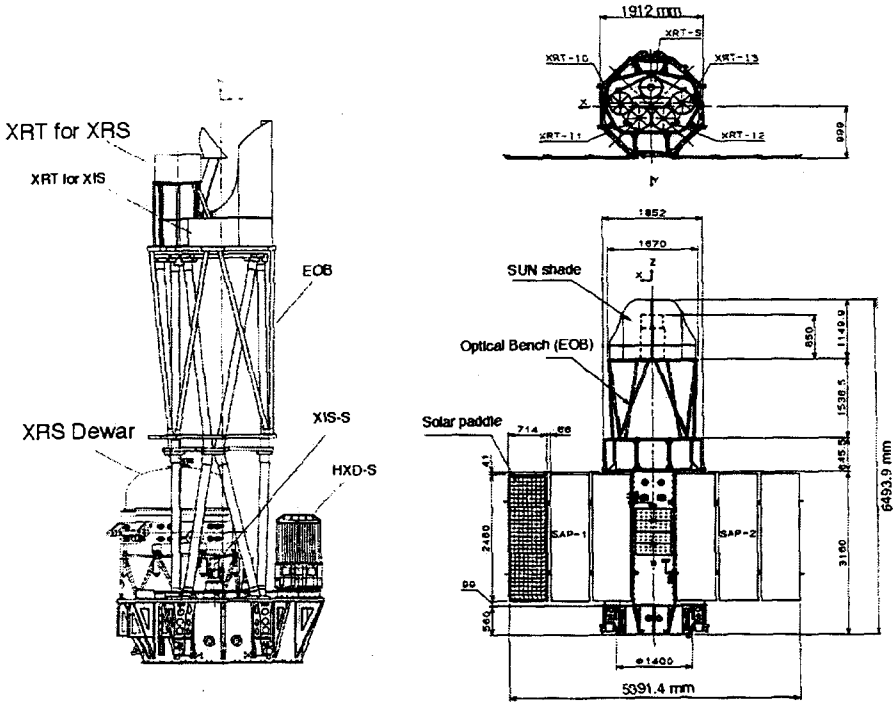

Figure 1. Schematic view of the Astro-E X-Ray Observatory. The X-ray mirrors are mounted on an extendable optical support structure that will be deployed in orbit.

The new capabilities afforded by Astro-E will enable the study of a wide range of high energy astrophysical sources with unprecedented spectral sensitivity over a combined bandwidth of 0.3 to 700 keV. The observatory will be launched into low earth orbit (550 km, 31° inclination) on a Japanese M-V rocket from the Kagoshima, Japan launch facility in early 2000. Operation of the observatory will be coordinated between the ground station at Kagoshima and ISAS. The XRS is a cryogenic instrument and is expected to last two years in orbit. Thereafter, the XIS will provide the basic imaging and spectroscopy function (between 0.3 and 12 keV) for the mission. Hence, the first two years of the mission will concentrate on investigations where the unique capabilities of the XRS are best suited. Nonetheless, a significant attribute of Astro-E is that all of the instruments are coaligned and powered on all of the time. This will provide a comprehensive picture of many celestial sources known to have very broad band X-ray emission. The international Astro-E Science Working Group will devote the first six months of the mission to deployment of the observatory, calibration and scientific observations. Thereafter, it will be open to guest investigators in Japan and the US on a competitive basis. Prospective investigators in other countries must coordinate their proposals through ISAS.

The key properties of the XRS in relation to other orbiting X-ray facilities are its energy resolution and collecting area for spectroscopy (Figure 2). The *Chandra* and XMM observatories will use transmission and reflection gratings for X-ray spectroscopy, which provide very high resolution at low energies. At higher energies, the dispersion of the gratings exceeds the (non-dispersive) resolution of the XRS, which has an energy resolution that is nearly independent of energy. The cross-over point is about 2 keV. The higher resolution and collecting area of the XRS make it the instrument of choice for studies in the 6 keV region, where the various states of neutral (cold) through highly ionized (hot) elements (particularly He- and H-like Fe) will provide a wide variety of diagnostic "tools" for inferring the conditions of the emitting gas. Further, the ability to centroid lines to the statistical precision of several eV at 6000 eV will allow velocities to be determined down to a few hundred km/sec. This will permit measurement of Doppler and turbulent motions that so far have not been available in the X-ray band. Thus, the Astro-E/XRS should sharpen our view of essentially all type of celestial X-ray sources and provide significant "discovery space" for revealing exciting new phenomena.

2. The XRS Instrument

The fundamental breakthrough in advancing high-efficiency, high-resolution X-ray spectroscopy came with the development of the X-ray microcalorimeter[6]. At very low temperatures (< 0.1 K), it is possible to construct a device with high responsivity and low thermal noise such that heat pulses from individual X-rays can be sensed and measured with a signal-to-noise of up to one part in several thousand. Of course real-world devices have limitations, such as additional noise terms (e.g., 1/f noise) and the limited availability of materials that thermalize X-ray efficiently without contributing excessive heat capacity. The goal of the XRS was to produce a microcalorimeter array with an energy resolution of 12 eV or better at 6 keV. The necessity for an array was set by the requirement to cover a useful field of view (~ 10 arcmin^2) yet remain within a heat capacity budget low enough to permit this resolution. Over a period of about a decade, work concentrated on producing devices that have this resolution with a high degree of uniformity over an array of 32 individual microcalorimeter pixels with size ~ 0.4 mm^2. For the XRS, the most straightforward path toward this was to use micromachined silicon as the basis of the array, with ion-implanted thermometer (i.e., a thermistor), and use the semi-metallic crystal mercury telluride (HgTe) as the X-ray absorber. Such devices are now capable of reliably producing an energy resolution of 12 eV at 6 keV with 95% absorption efficiency[7]. For an up-to-date review of X-ray microcalorimeters, including progress toward the next generation of devices, see Stahle, McCammon and Irwin [8].

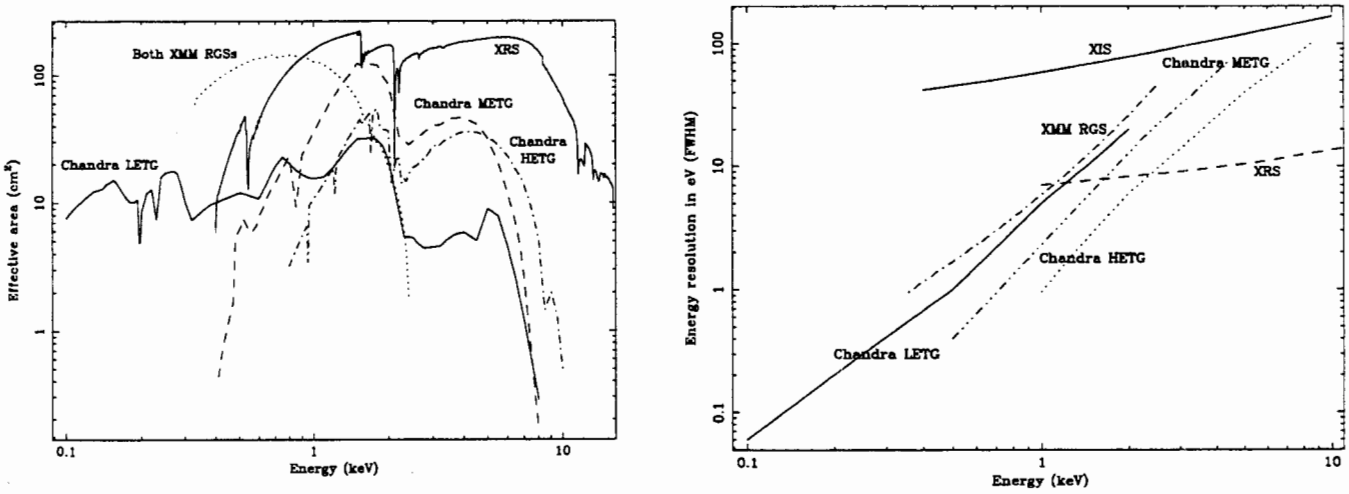

Figure 2. The effective area and energy resolution as a function of energy of the XRS in comparison with the X-ray spectrometers on the *Chandra* and XMM X-ray observatories. For energies above about 2 keV, the XRS has the highest collecting area for spectroscopy and also the highest resolution.

The implementation of a microcalorimeter spectrometer for use in space imposed a number of challenging requirements on the design of the instrument. Foremost among these was the necessity for cooling the device to 60 mK for a period of at least 2 years in order to carry out a reasonably comprehensive scientific observing program. This required a cryogenic system with extremely low heat loads that was engineered for spaceflight and small enough to fit within a restrictive envelop (< 1 m^3). To meet these constraints, a three stage cooling system was developed jointly by Goddard, the University of Wisconsin, ISAS, and the Sumitomo Heavy Industries Corporation (SHI). The detectors are cooled to the operating

temperature with a conventional single stage adiabatic demagnetization refrigerator (ADR; see Porter et al.[9]). The ADR is suspended within a 1 tesla/amp superconducting magnet that is immersed in a 32 liter liquid helium cryostat. The He will be pumped by space to about 1.3 K (which means that it will be in its superfluid state) and essentially serves as a heat sink for the ADR. To achieve the design goal of a 2.5 year lifetime, a net heat load into the He cryostat of less than 1.2 mW was required assuming the cryostat is 90% full at the beginning of the mission. The He cryostat is mounted within an annular dewar that will contain solid neon, which will also be space-pumped to a temperature of about 17 K. Careful attention to thermal isolation, controlling superfluid film creep, heat sinking and staging of components to minimize parasitic heat loads was required simultaneously with the need to keep the system as modular as possible, and survive the demanding launch loads. The responsibilities for the components of the XRS (Figure 3) were shared between the US and Japan, and included many institutions. The He Insert, consisting of the He cryostat, ADR, detector assembly, blocking filters and instrument electronics were the responsibility of Goddard. The University of Wisconsin supplied the flight ADR salt pill. The Ne dewar was developed at SHI under the direction of ISAS. The other electronics boxes (power and telemetry/commanding) were provided through ISAS, and the filter wheel was developed at the Tokyo Metropolitan University and ISAS. The ground calibration of the instrument was done primarily at Goddard with assistance from ISAS.

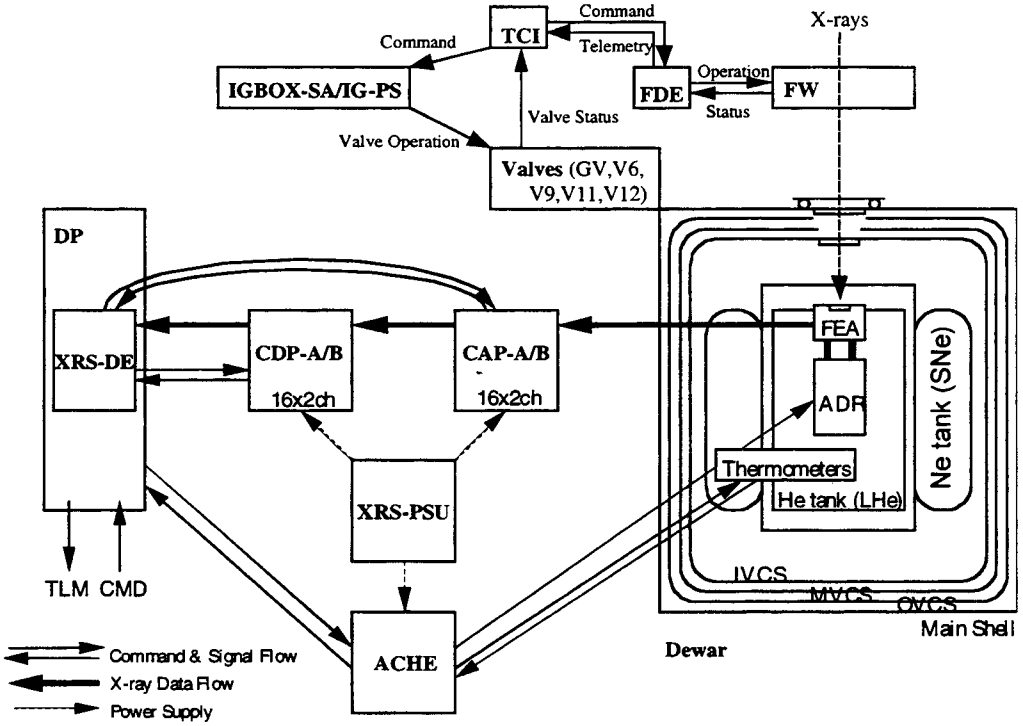

Figure 3. Block diagram of the XRS Instrument. The CAP and CDP are the analog and digital processors, and the ACHE provides ADR control and thermometer readout. The PSU provides power to the individual boxes and the DE handles commanding and telemetry. The filter wheel is attached to the spacecraft structure just above the dewar gate valve and is separately operated.

The microcalorimeters are by their nature highly sensitive to essentially all forms of electromagnetic and particle radiation, so proper isolation from structures at higher temperature was necessary. This required the development of aluminized plastic filters that are thin enough to transmit X-rays yet strong enough to survive a few torr of differential pressure, repeated thermal cycling to cryogenic temperatures, and substantial random mechanical vibration.

In the following sections we will successively go through the major components of the XRS, starting with the detector array and ending up with the electronics, and then discuss the performance of the XRS.

2.1. Microcalorimeter Array

The microcalorimeter works by sensing the energies of individual X-ray photons as heat. The device consists of an X-ray absorber attached to a thermometer. The thermometer and absorber are in turn connected to a heat sink through a low

conductance link for thermal isolation. The temperature rise is given approximately by $\Delta T \sim E/C$, where E is the energy of the photon and C is the heat capacity of the sensor. The thermal recovery time is given by $\tau \sim C/G$, where G is the thermal conductance to the heat sink. Since the heat capacities of materials generally decrease with temperature (either as T or T^3 for metals and crystalline dielectrics, respectively), and thermal fluctuations also scale with temperature, the device must be cooled to temperatures below 0.1 K in order to work as a thermal sensor. The heat capacity and thermal conductance of the XRS detector are $\sim 2 \times 10^{-13}$ J/K and 2×10^{-11} W/K, respectively, at the temperature of the sensor under bias (~ 75 mK). The actual response of the detector is somewhat more complicated, due to electrothermal feedback (a change in the pulse recovery time caused by the variation in ohmic power dissipation in the thermistor as its resistance changes) and the physics of X-ray thermalization. Theoretically, a calorimeter with a resistive thermometer should only have phonon noise and Johnson noise, and an energy resolution of a few eV should be possible with established materials and assembly procedures. The signal response should be linear with energy to the extent that $\Delta T/T$ is small. In practice, there are non-ideal effects that limit the resolution of the XRS array to about 12 eV (at 6 keV). Nonetheless, this is still an order of magnitude lower than has been available in a high efficiency X-ray spectrometer.

The microcalorimeter sensor for the XRS is based on micromachined, ion-implanted silicon thermometers and separately attached HgTe absorbers[7,10]. The temperature-sensing element has an electrical resistance that increases rapidly with decreasing temperature. By applying a bias current through the sensor, the voltage drop generated by the absorption of a single X-ray can be easily measured. Basically, a silicon wafer is successively patterned, ion-implanted, and etched to form thermally isolated pixels. The photolithographic masks are designed to produce two linear rows of pixels. Each pixel has three beams, two for read out via degenerately doped Si (with phosphorous) and a third beam strictly for mechanical support. The array is laid out such that the two rows are opposite each other, with the third beam passing in between the pixels on the opposite side (Figure 4). After screening the finished arrays for thermometer sensitivity, silicon spacers are attached with epoxy to each pixel element and then HgTe die are attached, again using epoxy. The Si spacers help prevent the epoxy from wicking beyond the spacer due to surface tension effects and keep the overhanging absorbers from touching the support beams. The thermalization of X-rays over a broad bandpass requires X-ray absorbers that are optically thick, convert X-rays into heat in a manner that is describable with a single kinetic temperature at any time, and have a heat capacity low enough to allow the specified energy resolution. The "zero-energy bandgap" semiconductor crystal HgTe provides these attributes reasonably well. The absorbers are purposely cut to a size that provides a high filling factor and covers the silicon pixel and support beams as much as possible. The HgTe has a thickness of about 8 microns and each pixel measures 1.23 × 0.32 mm (57" × 15" on the sky); the filling factor of the flight array as assembled is 95%.

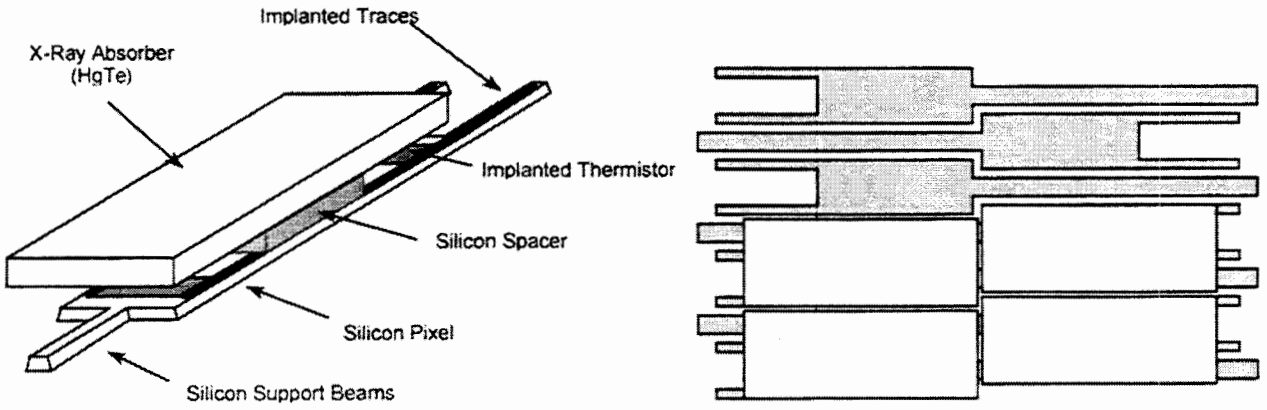

Figure 4. Schematic of the XRS microcalorimeter array, showing the assembly of a single pixel and the "tiling" of the array with the absorbers.

2.2. *Detector Assembly*

Microcalorimeters with thermometers based on doped semiconductors generally have electrical impedances in the range 10's to 100's of MΩ. With such a high impedance, the effects of coupling capacitance to the dewar over long wiring runs would lead to prohibitively high susceptibility to microphonics. To avoid this problem a simple JFET source-follower circuit is employed to transition from the high impedance of the detector to the much lower output impedance of a JFET, which is of the order of 1 kΩ. The basic circuit is straightforward to implement. The version for the XRS is shown in Figure 5. One complication that arises is that the JFETs must remain above ~ 100 K in order to prevent charge carriers from freezing out.

This requires careful thermal staging of the JFETs in order to minimize their heat load on the He cryostat and also prevent their thermal emission and conducted heat from reaching the detector stage.

Because the detector resistance has a negative temperature coefficient, it is desirable to bias the detector with fixed current in order to achieve negative electrothermal feedback (i.e., $dP/dT < 0$, where $P = I^2R$). This is done (to a good approximation) with the 90 MΩ load resistor in series with the detector, which operates at about 10 MΩ under a nominal bias voltage of 1.74 V applied to the bias circuit. The voltage divider circuit involving the 1 MΩ, the 100 kΩ, and the 10 kΩ resistors shown in Figure 5 is designed to attenuate noise (by a factor of 100) that couples in on the bias lines between the mainshell and the 17K interface, and between the 17K interface and the detector assembly (by a factor of 10). For redundancy, the bias circuit is actually divided up into four groups of 8 channels each. The 1 MΩ resistors are heat sunk at 17 K in order to avoid dissipating ohmic power to the He tank (about 9.8 μW total). The other resistors only dissipate about 1 μW to the He tank. The 2 kΩ resistors are inserted in the output return lines (one for each channel) in order to approximately balance the output impedance of the JFETs for the differential preamplifier of the analog electronics outside the dewar.

The front end detector assembly (FEA) contains the detector and front end electronics. The basic requirements on the FEA are to isolate the detector from non-X-ray power (down to a level of ~ 10^{-14} W/pixel), support all of the thermally isolated components to withstand mechanical launch loads, and prevent low level vibrations from exciting resonances in the wiring between the detector array and the JFETs. The basic approach was to mechanically support the detector housing and the JFET assemblies with Kevlar because of its excellent strength/thermal conductance ratio, and use tensioned electrical wires to obtain resonant frequencies well above the excitations due to launch vibrations, momentum wheels and gyros. The FEA also needed to be kept as modular as possible, with separate assemblies for the detector, JFETs and biasing electronics. The connection of the detector housing to the ADR is made with annealed gold straps to provide adequate thermal conductance.

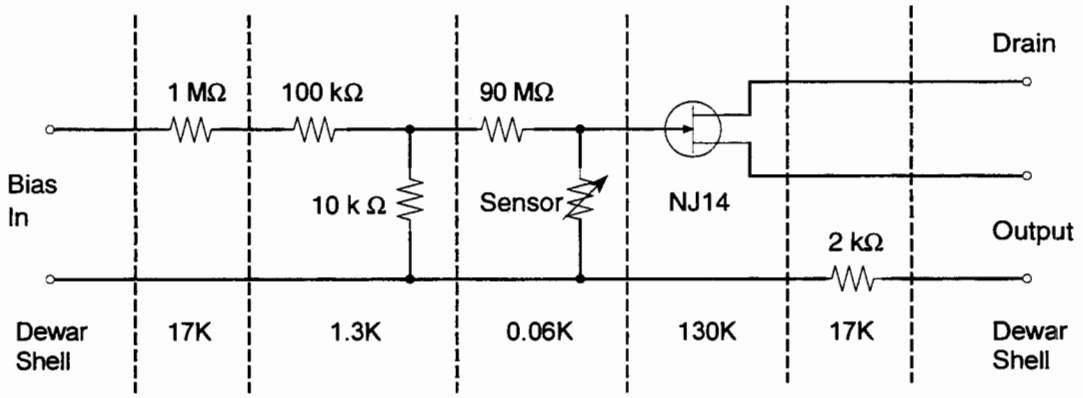

Figure 5. The basic circuit for biasing and reading out the XRS microcalorimeter. The source-follower circuit is employed to transition from the high impedance of the detector to the much lower output impedance of the JFET, thus lowering the susceptibility to microphonics in long wire runs. The temperature of each stage is indicated.

The FEA is shown schematically in Porter et al.[9] The bias box houses the 100 kΩ and 10 kΩ dividing resistors, provides the connector interface to the thermometers on the detector housing, and provides a low resistance connection to the detector in order to provide a reference ground for the analog electronics outside of the dewar. The detector housing, designated the Calorimeter Thermal Sink (CTS) supports the load resistors, four RuO_2 thermometers, the microcalorimeter array and the anticoincidence detector[7]. The load resistors are thin-film NiChrome die attached to a high purity alumina board with epoxy. Each channel has three 30 MΩ resistors wire bonded in series to give 90 MΩ. The board is fastened to the underside of the copper CTS. Inside the detector box, the array and anticoincidence detector are mounted on separate high purity alumina boards and stacked. The detector board has a rectangular cut-out under the array to allow the anticoincidence detector to sit up underneath the array. This is to minimize the distance between the anticoincidence detector and the array in order to maximize the geometrical anticoincidence rejection factor. The CTS has two gold-plated alumina feedthrough blocks with buried traces that are epoxied in place with silver-filled epoxy to prevent light leaks. The lid to the CTS fits with a tongue-and-groove arrangement and contains two radioactive isotopes, ^{41}Ca and ^{55}Fe, that illuminate the array with 3.3 and 3.6 keV, and 5.9 and 6.4 keV X-rays, respectively. These are used to provide absolute monitors of the detector gain throughout the mission. The fluxes from these sources were chosen to be high enough to use for long-term (> 10 minutes) gain corrections, but low enough to not significantly interfere with the X-rays from celestial sources. The rates from the two sources are

different on the two sides of the array due to partial shadowing by the detector "beam blockers". One side of the array (lengthwise) has 0.25 and 2×10^{-3} cps/pixel from ^{41}Ca and ^{55}Fe, respectively, and the other side has 0.03 and 0.01 cps/pixel, respectively.

Kevlar yarn with a gauge of 195 denier (~ 7-8 lb. instantaneous failure limit) was used for the suspension of the CTS and the Inner JFET Box. Kevlar yarn with a gauge of 55 denier (~ 2 lb. instantaneous failure limit) was used to support the JFETs within the Inner Box. The suspension system was designed to withstand static loads of 35 g in the thrust axis and 15 g in the lateral direction. The resonant frequencies were chosen to be in a range where there is relatively little vibration input transmitted to the He cryostat. The suspension system is configured in such a way that the Young's modulus of the Kevlar and the mass of the suspended element determine the resonant frequency, which is about 300-350 Hz. The engineering model was successfully tested to 8.5 g_{rms} and 24.5 g shock in the thrust axis and 5.0 g_{rms} and 9 g shock in the lateral axes. The flight model was tested to comparable levels. The CTS makes thermal contact to ADR through four flexible gold straps that were annealed prior to assembly. This was done to minimize the mechanical coupling between the two structures since the ADR suspension has a lower resonant frequency.

2.3. ADR

The ADR is used to cool the detector array to 60 mK. This cooling technique was adopted because of its simplicity and suitability for spaceflight use. No moving parts or gravity are required for operation. Briefly, the ADR works by using a system of magnetic spins with interaction energy much lower than kT at ~ 1K to exchange the entropy of an ordered system of spins at higher temperature for that of a relaxed system at lower temperature. The spins are aligned using an external magnetic field (~ 1.6 tesla averaged over the ADR salt pill) and the heat of magnetization is conducted away to the He bath through the heat switch. This lowers the entropy of the spin system isothermally. The heat switch is then opened and the magnetic field is reduced, causing the spins to demagnetize adiabatically, and the system to cool. In practice, the magnetic field is ramped down to a finite value such that the temperature of the saltpill is 60 mK, and the remainder of the cooling power is used to regulate the temperature at this value for an extended period of time.

The ADR is comprised of 917 grams of ferric-ammonium sulfate paramagnetic salt in a hermetically sealed stainless steel container developed at the University of Wisconsin[9]. The overall size of the salt pill was originally set by the need to provide operation at 65 mK for 24 hours with a duty cycle of about 95%. This implies an ADR "recharge" time of about one hour. The ADR heat switch is a He gas-gap heat switch filled with ^3He to 1.14 atm gas at room temperature. The switch consists of a series of nested copper cylinders acting as a heat exchanger. The cylinders are alternately connected to the hot and cold ends of the switch. When cold (< ~ 9 K), the ^3He gas is adsorbed in a separate volume containing about 1 gram of Zeolite pellets that getter the helium. The volume containing the Zeolite is connected to the body of the switch through a thin-walled stainless steel tube for appropriate thermal isolation. To close the switch, heat is applied to the getter, which drives the ^3He gas out and into the heat exchanger volume. To open the switch, the heater power is disabled and the getter cools and re-adsorbs the He.

The procedure for operating the ADR is straightforward. Current is applied to the magnet and made to ramp up at a steady rate. The heat switch is then is closed by applying current to the getter heater. The magnet current is ramped up to its ultimate value of 2 amps. During this time the salt pill heats up to about 1.8 K and then cools back down close to the He bath temperature (about 1.3 K) as the heat of magnetization is conducted through the heat switch to the He cryostat. Once this happens, the getter heater is turned off, allowing the heat switch to open. The magnet current is then ramped down close to a value of about 45 mA, corresponding to a temperature of 60 mK, and then the system goes into closed-loop temperature control. This entire process takes about 65 minutes. In the course of developing the XRS, the performance of the ADR has been improved. It is now expected that the hold time at 60 mK will be about 36 hours in orbit, including a conservative estimate of cosmic ray heating of the salt pill. The temperature is controlled by feeding the error signal from a thermometer measurement of the CTS to the magnet current supply. A temperature stability of better than 10 μK (rms) has been achieved with this system, which makes a negligible contribution to the energy resolution of the detector.

The magnet is essentially a ~ 1 kH solenoid of (superconducting) NbTi wire immersed in the He cryostat. The magnet was fabricated by Cryomagnetics Corporation and produces very close to 1 tesla/amp at the center. The magnet has active shielding (bucking coils) to reduce the external magnetic field. The hysteretic losses from operating the magnet have been empirically determined to be about 6.8 Joules for a single ADR cycle[11].

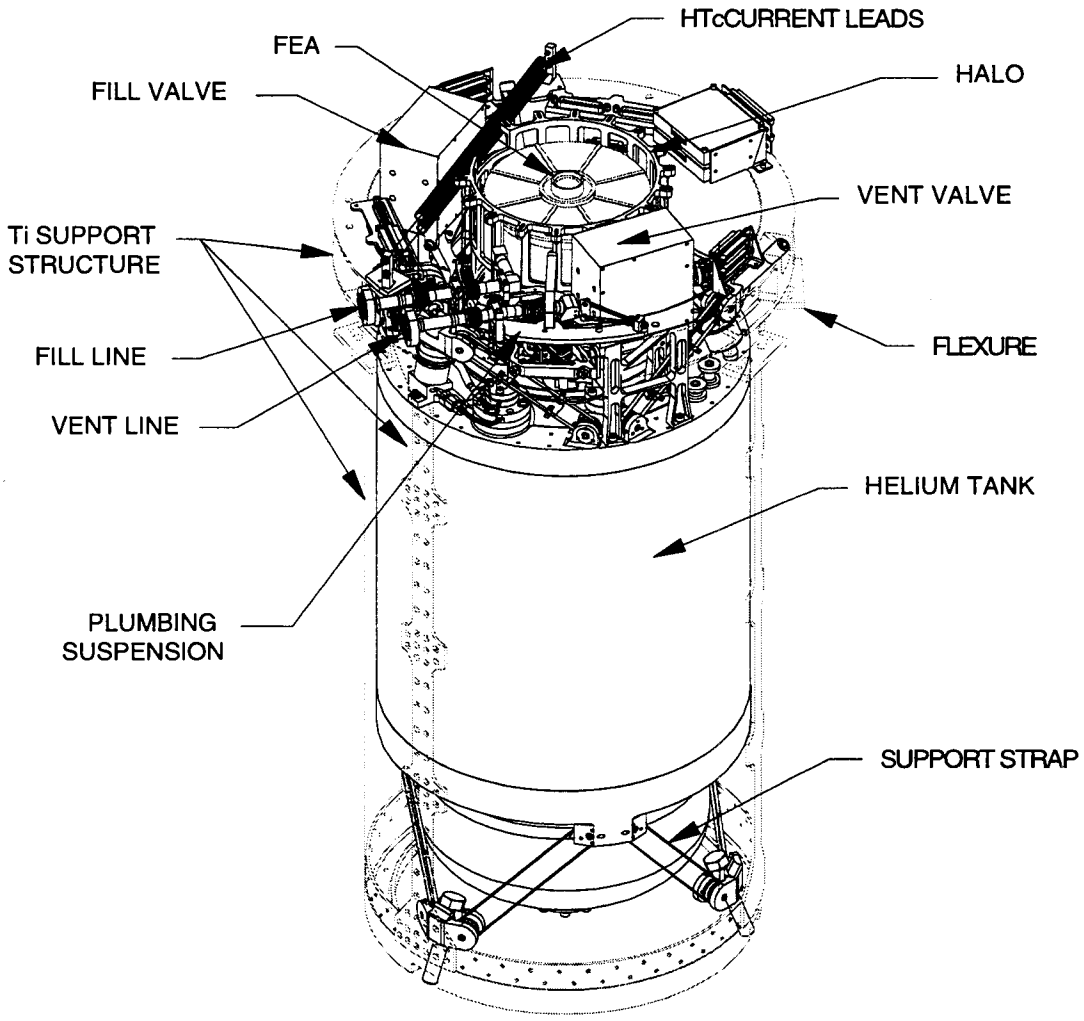

Figure 6. Schematic view of the XRS He Insert showing the principal components.

2.4. He Cryostat

The He cryostat serves mainly as a heat sink for the ADR and the detector system, and also for one of the 5 blocking filters. The cryostat system must contain the superfluid He, support the ADR magnet, salt pill, heat switch, detector assembly, cryogenic valves and valve motors, and survive all of the prelaunch thermal cycles, vibration tests and launch loads. The heat load requirement for meeting the 2.5 year lifetime goal is ~ 1.2 mW. In order to achieve a value this low, a number of cryogenic engineering innovations had to be developed (see Breon et al.[12] and references therein). One of these was the development of low thermal conductance leads to supply current to the ADR magnet (2 amps maximum) and cryostat valve motors with minimal heat load[13]. Wire with a gauge sufficient to handle 2 amps of current would lead to a prohibitively high heat load between 17 K and 1.3 K. This problem was solved by employing a high temperature superconductor. Fibers of YBaCuO are bonded to a fiberglass tube that is suspended using Kevlar braid. One end is heat sunk to the 17 K interface and the other is heat sunk to part of the helium vent line that is at ~ 4 K. There are two such structures for redundancy. Another serious (effective) heat load was the flow of superfluid helium out the cryostat vent line. Superfluid helium tends to flow in the direction of a thermal gradient. This problem is significantly reduced by using a porous plug that sets up an inverted temperature gradient at the cryostat exit. The design of the cryostat vent line has three major components to reduce superfluid flow. These are a small porous plug, a heat exchanger, and an etched Si "knife edge" film killer[14]. The heat exchanger provides a higher temperature just outside the vent so that helium gas leaving the porous plug does not re-condense. The film killer should provide an effective backup should the thermodynamic conditions in the vent line be different in orbit.

The heat loads on the He cryostat have been measured and found to be in good agreement with a detailed thermal model of the He Insert[11, 12], and are in fact sufficiently low that the goal of 2.5 years could be reached with significant margin. Of course the He cryostat heat loads are low only if the Ne tank is at 17 K. Similarly, the net heat load on the Ne dewar depends in part on the cooling of shields from the cold helium gas vented from the cryostat. Thus, the lifetimes of the two cryogens are coupled. The He cryostat has been tested with and without the FEA and ADR, so the heat loads from these components have been reliably determined. The heat load on the cryostat without the ADR and FEA is about 629 μW. The FEA alone adds another 95 μW with the JFETs powered on. The time averaged heat load from the ADR is about 155 μW. When incorporated into the cryostat, the net heat load, after taking into account the effects of vapor cooling from the additional heat load, is only 784 μW. Assuming the 32 liter He tank is 90% full after reaching orbit, this gives a formal lifetime of 3.7 years (again, assuming the interface to the He cryostat were maintained at 17 K at least this long). This indicates excellent performance of the cryostat and provides considerable margin for maintaining the two year lifetime requirement against additional heat loads or problems (e.g., a thermal short or loss of cryogen on ascent). In principle, the additional margin on the helium lifetime could be used to operate the ADR at a lower temperature to enhance the detector performance. The He cryostat is equipped with a heater for mass gauging the liquid helium[15]. A small amount of heat is dissipated in the helium and the resulting temperature rise is measured. Knowing the heat capacity of helium one can determine the volume of helium remaining. This will be extremely useful for optimizing the long-term mission planning.

2.5. Neon Dewar

The Ne dewar intercepts the substantial heat load from the warm mainshell of the dewar and provides a heat sink for plumbing lines, wiring and other components, such as the JFETs. The dewar was designed and developed by the Sumitomo Heavy Industries Corporation and ISAS[16]. In order to facilitate the dual cryogen design, the Ne dewar and He Insert had to have a simple and robust interface. As with the He cryostat, every effort was made to keep the heat loads into the neon tank as low as possible. In particular, the support straps were optimized for mechanical strength and minimum thermal conductance. Mechanical shock absorbers were added to the dewar support structure to reduce the mechanical load on the straps, thus allowing straps with smaller cross section. The Ne dewar consists of an annular aluminum vessel with a volume of about 130 liters. The aluminum tank is suspended on S-glass fiber-reinforced polymer straps from the aluminum mainshell. The tank is filled with an aluminum foam with a 3% filling factor to add structure to the solid neon and help keep the tank isothermal as the neon sublimates away. The present estimate of the neon lifetime is about 1.91 years. This will be the limiting factor in the XRS lifetime, but as mentioned above, maximizing the overall cryogen lifetime requires optimizing vapor cooling, and this has not yet been carried out on the flight system.

2.6. Blocking Filters

The blocking filters are a fundamental component of the XRS. Basically, the filters prevent radiation with wavelengths longer than X-rays from reaching the detector, where it would heat up the pixels or induce photon shot noise. The filters also close out the various thermal shields of the dewar to minimize heat loads on the cryogens. The driving factor in the design of the filters was the need to keep the geo-coronal radiation line (304 Å) from reaching the detector. There are other stringent requirements on the longer wavelength UV, visible and IR rejection, but with the basic design of the XRS filters (five filters in series), these are easily met once the geo-coronal emission is appropriately attenuated. These requirements set the minimum total thickness of the filters, but there are other factors that had to be included as well. These were the need to survive numerous thermal cycles to very low temperatures, mechanical vibration, pressure gradients of a few torr, and be sufficiently non-permeable to water vapor at room temperature. Through years of testing, and feedback with the manufacturer of the filters, Luxel Corporation, we arrived at the filter parameters shown in Table 1. The filters are aluminized polyimide[17] and are highly reflective in the visible and IR. The UV attenuation is determined by both the aluminum and polyimide thicknesses.

The design qualification program for the engineering model filters consisted of white light transmission tests, three thermal cycles, and two additional thermal cycles to low temperature as part of vibration tests (30 sec and 90 sec, respectively) in a vibratable dewar. The flight filters were accepted if they passed a white light transmittance test, one thermal cycle, and another as part of a 30 sec cold vibration test. Once installed in the flight dewar, the filters (particularly the CTS filter) are subjected to additional thermal cycles and vibration tests prior to launch. A plot of the quantum efficiency, defined as the transmission of the five filters multiplied by the absorption efficiency of the detector, is shown in Figure 7.

Table 1 - Properties of XRS Blocking Filters

Filter	Nominal Temperature (K)	Polyimide Thickness (Å)	Aluminum Thickness (Å)
Dewar Mainshell†	250	1000	800
IVCS	124	1000	1000
Neon	17	1000	1000
FEA	1.3	750	500
CTS	0.06	750	500
	Totals:	**4500 Å**	**3800 Å**

†Filter is mounted on a Ni mesh (70 lines/inch) that is about 78% open geometrically. The mesh structure is about 0.001 inches thick.

Once the flight dewar assembly was finished, the aperture cylinder was installed. The main purpose of the aperture cylinder is to prevent outgassing water vapor from the warm outer layers of dewar multilayer insulation from reaching filters that are cold, where it could condense to form ice. The aperture cylinder and Ne dewar vapor-cooled shields combine to provide a labyrinth path between the main shell, the outer, and the middle vapor-cooled shields. The back end of the aperture cylinder is free mechanically but has a thermal heat strap that is attached to the Inner Vapor-Cooled Shield (IVCS) of the dewar. In the event that water ice is a problem, the IVCS and mainshell filters are equipped with heaters than can be used for "defrosting". The heater values are 0.33 and 0.75 W for the IVCS and mainshell filters, respectively. With the aperture cylinder in place, the four remaining filters were installed in succession, starting with the FEA filter. (The filter on the CTS is attached directly to the lid and was installed and protected earlier in the integration of the instrument.) A special tool was used to load and lock the filters into place. Once the mainshell filter was installed, the dewar gate valve was attached and the dewar guard vacuum was pumped out for 5 weeks. The dewars were then filled with cryogen for testing.

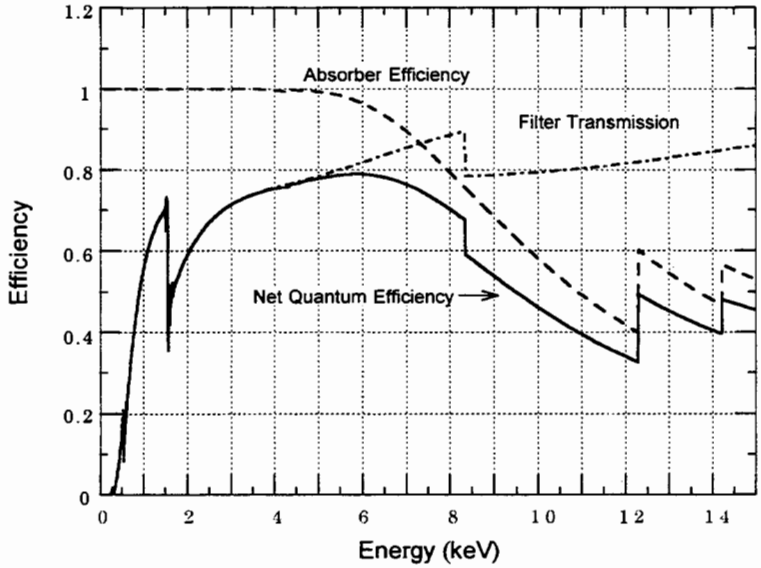

Figure 7. The quantum efficiency of the XRS as a function of energy. The plot does not include any effects due to the point-spread function of the mirror system.

2.7. Instrument Electronics

There are three main electronics boxes associated with the XRS. The Calorimeter Analog Processor (CAP) provides power to operate the JFETs and controls their temperature to a specified value (typically 130 K), and amplify all of the calorimeter signals with a gain of 20,000. There is a dedicated amplifier chain for each channel. The basic front end of the amplifier is a differential discrete pair of low noise InterFet IFN146 JFETs. The amplifier stage was designed at Goddard and fabricated in small (~ 1 × 2 inch) thick-film hybrid packages by Teledyne. Particular attention was paid to keeping the susceptibility of the amplifier gain to temperature variations as low as possible.

The calorimeter digital processor (CDP) provides all of the pulse height processing electronics and communication with the telemetry electronics[18]. The analog voltages from each channel are digitized at 12,288 Hz (a 16,384 Hz rate is also available) and then algorithms are employed to detect and flag pulses. A key feature of the CDP is the ability to digitally compute pulse heights on the basis of optimal coefficients generated from the *in situ* noise spectrum and pulse shapes. This allows for optimal performance under actual flight conditions. The coefficients can be computed on board or on the ground on the basis of data previously recorded, and then uploaded. As the count rate from a source increases, the resulting pulse pile-up will eventually compromise the pulse height determination. To deal with this, the CDP processes events differently according to their relation in time to other events. There are three "grades" of events, high, mid, and low, depending on the relative inter-pulse arrival times. This results in a larger fraction of events with high resolution. These grades are recorded with each event and the user can specify which are to be used for analysis. The CDP also computes pulse rise times, which will be used to distinguish between events absorbed in the HgTe absorber of each pixel from those absorbed in other parts of the detector, flags events if they occurred in coincidence with the anticoincidence detector, and determines the pulse arrival times to a precision of ~ 10 μsec.

The ADR Control and Housekeeping Electronics (ACHE) performs all of the functions necessary to operate the ADR and readout of the thermometers from both the He Insert and Ne dewar. The cycling of the magnet is performed in software and can be tailored to optimize the performance of the cycle. Once the operating temperature is reached, the unit transfers control to a hardware temperature controller. Either one of the two thermometers on the CTS can be used for closed-loop temperature control. The error signal is feed back directly to the current supply of the magnet.

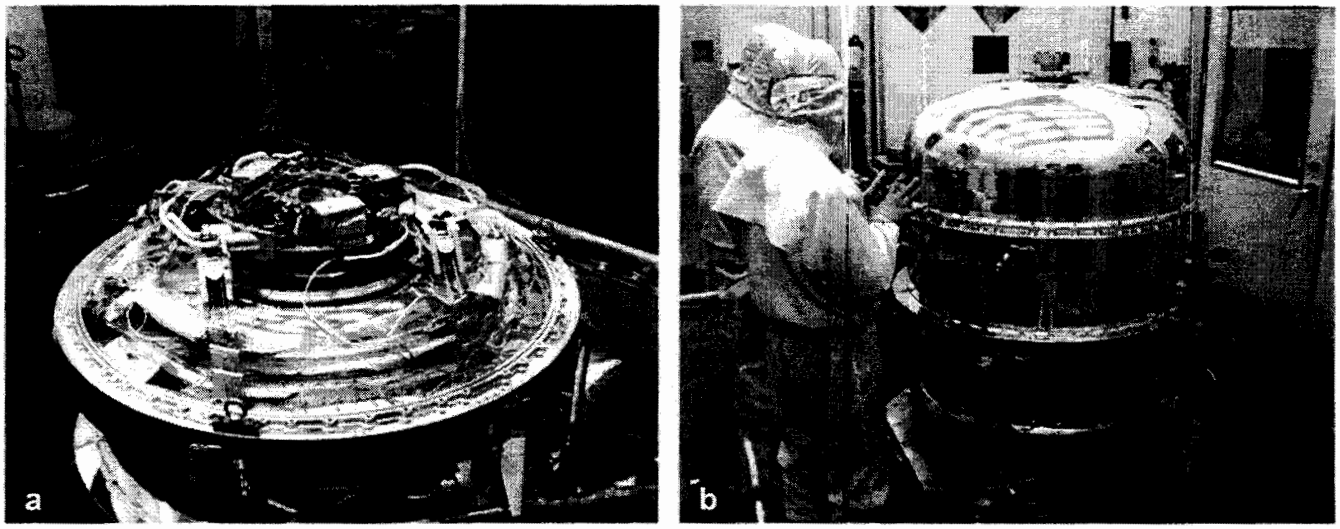

Figure 8. (a) The forward end of the XRS dewar showing the He Insert installed in the Ne dewar. The top of the Ne tank, support straps and vapor-cooled shields are visible. (b) XRS dewar closed out for operation.

2.8. Filter Wheel

The filter wheel was incorporated into the design of the XRS so that the relatively bright sources (> 50 mCrab) could be observed without excessive pulse pile-up. The wheel was developed mainly at the Tokyo Metropolitan University and ISAS[19]. The wheel is mounted just above the gate valve and there are six positions in the wheel. Three have neutral density filters, consisting of 200 μm thick molybdenum foils with a uniform pattern of small holes, two "soft cut-off" filters made from Be foil, and, of course, an open position that will be in place at launch. The neutral density filters provide throughputs of 5%, 10% and 25%. The Be foils are 100 μm and 300 μm thick. The soft cut-off filters are for observations where the flux at 6 keV is of primary importance and the flux at lower energies can be sacrificed so as to insure that a higher fraction of the events will be flagged as high- and mid-resolution by the CDP. These filters can be characterized by the energy at which the throughput drops to 50%. These energies are approximately 2.5 keV for the 100μm filter and 3.5 keV for the 300 μm filter.

3. Instrument Characteristics and Performance

The XRS Insert was completed and installed in a test dewar in December 1998 for a final checkout and calibration prior to shipment to Japan. Vibration tests at 77K and electromagnetic interference and compatibility tests were successfully conducted earlier in the year. The test dewar was designed with a simulated Ne dewar interface. A set of flight-like engineering model blocking filters was installed and the system was then pumped down and cooled to operational temperature. A description of the filter calibration program is given by Audley et al.[20] The first activity was to determine the proper thresholds for pulse triggering by the CDP. Then the optimal bias point was determined by recording data at a series of bias voltages, computing optimal coefficients at each bias, and determining the energy resolution using ^{55}Fe. A number of tests were carried out to measure heat loads, susceptibilities of the detector to various temperatures in the dewar, and visible light from outside the dewar. The performance of the anticoincidence detector was also verified. Following these tests a series of crystal and grating monochromators were used to measure the response of the detector system to monochromatic X-rays[21]. The primary objective was to determine the spectral redistribution function (which includes the energy resolution) of the detector.

The energy resolution of the flight array is typically 8-11 eV (FWHM) at 3.3 keV and 10-14 eV at 6 keV, so the basic goal of achieving 10-12 eV resolution with the XRS has been realized. The response to monoenergitic X-rays is mostly gaussian, but there is a tail to low energies and also broadening on the high-energy side. The low energy tail can be accounted for by electrons that are produced in the course of the thermalization process that have enough energy to leave the surface of the absorber (i.e., continuum escape events). The high-energy tail, which is confined to a few FWHM or so of the peak, is not well understood yet. The fraction of counts in the tail varies from pixel to pixel. There are indications that the fraction of events in this tail depends on where the X-rays are absorbed within the pixel, so it is reasonable to believe that they are associated with variations in the thermalization depending on where the X-rays are absorbed relative to the silicon spacer. This effect will be studied further with calibration of a spare detector system.

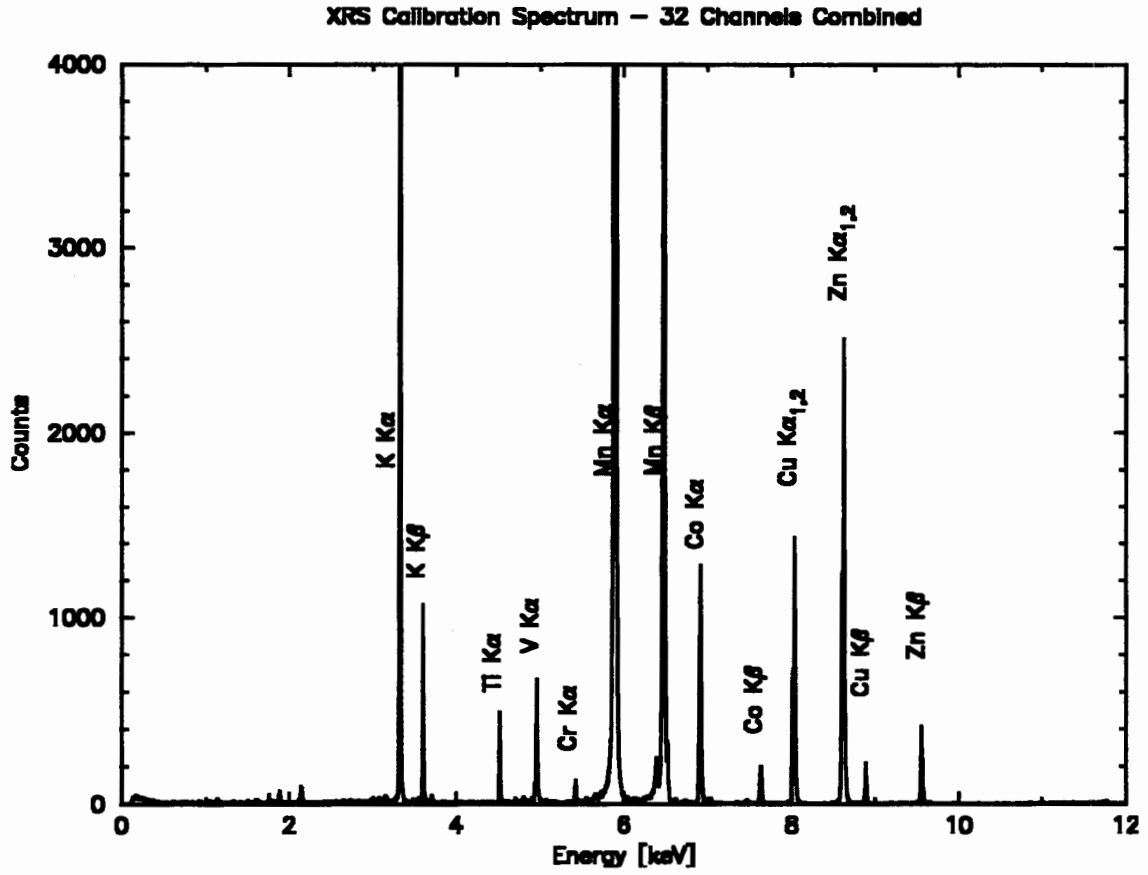

Figure 9. Pulse height spectrum obtained with the XRS from a series of electron-beam fluoresced targets. The spectrum includes all 32 channels. The instrument was running at its nominal operating temperature of 60 mK.

Another important quantity measured was the pulse height-energy gain. This was done by placing a number of targets on positions of a wheel and rotating the wheel past an X-ray beam to produce characteristic X-rays. In this way the entire spectrum was measured every 15 seconds to prevent long-term gain variations from leading to systematic energy gain errors. These measurements were repeated at a series of temperatures so that we could develop a model of how the gain scales with temperature should we choose to run the XRS at some temperature other than 60 mK. Figure 9 shows the results of the instrument response at 60 mK. All 32 channels of the instrument were combined for this spectrum.

Finally, to illustrate the power of the Astro-E/XRS for celestial X-ray spectroscopy, we show the expected spectrum from an X-ray emitting cluster of galaxies (Figure 10a). Such objects are emission line-rich from a full range of ionized elements in the hot intracluster medium. They are key to the study of the origin and evolution of the universe because of their immense volume and the large amounts of dark matter they are inferred to contain. The simulation is of a 100 ksec exposure of the Centaurus cluster of galaxies. Lines from a cooling flow component and the 3.2 keV isothermal component are clearly seen throughout the spectrum. The He-like triplet of iron, redshifted down in energy by about 70 eV, is also easily detectable (Figure 10b), and will provide sensitive diagnostics on the physical conditions within the cluster medium. A number of such objects will be observed with Astro-E, covering a range epochs (redshifts).

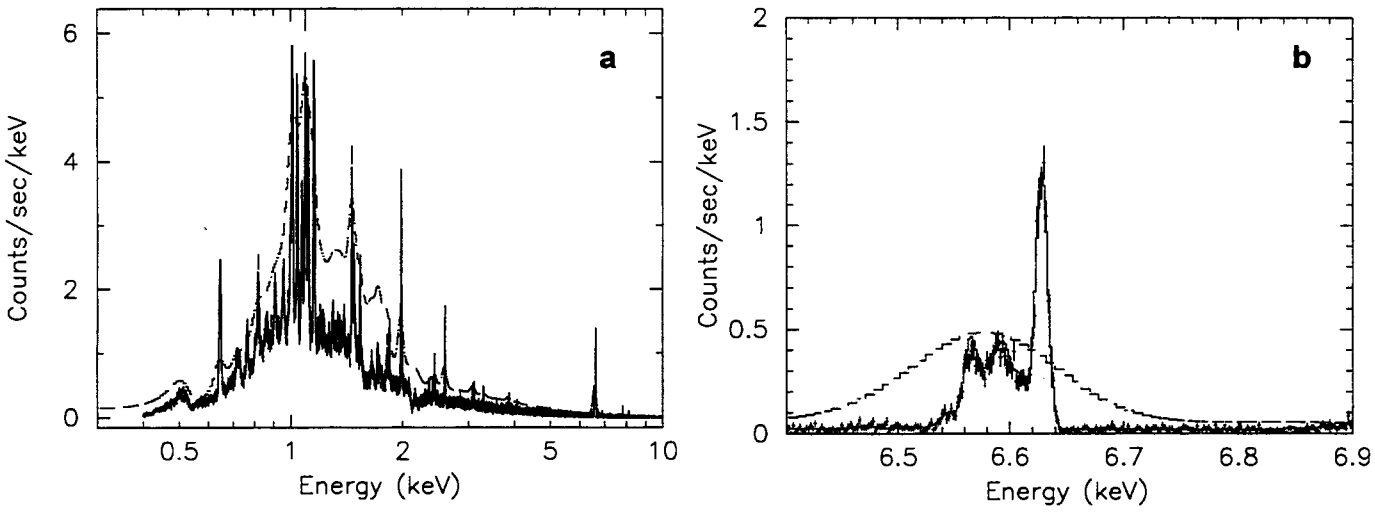

Figure 10. (a) Simulation of a 100 ksec exposure of the Centaurus cluster of galaxies with the XRS showing the spectrum over the full range of the instrument. The simulation assumes that the cluster is centered on the array. (b) Portion of the spectrum showing the Fe-K complex. In both plots, the best-fit model to only one of the four XIS spectra is also shown for comparison.

ACKNOWLEDGEMENTS

The authors are extremely grateful to a great many people at the Goddard Space Flight Center, the University of Wisconsin and the Institute for Space and Astronautical Science in Japan for their tireless efforts in bringing the XRS to fruition. The Luxel Corporation has also contributed greatly to the design and reliability of the blocking filters. The authors are particularly grateful to Profs. Yoshiaki Ogawara and Hajime Inoue at ISAS for their continuous help and support of the XRS. We would also like to extend appreciation to Mr. Masayuki Hirabayashi and his team at the Sumitomo Heavy Industries Corporation for their hard work on the Ne dewar and integration of the XRS.

REFERENCES

1. Y. Ogawara, "The Astro-E Mission", *IAU Symposium*, **188**, pp. 75-78, 1998.
2. H. Inoue, "The Astro-E Mission", *Proc. Of the 11th Colloquium on UV and X-Ray Spectroscopy of Astrophysical and Laboratory Plasmas*, Universal Academy Press, p. 239, 1995.
3. H. Katayama, M. Shouho, K. Katayama, T. Kohmura, K. Yoshita, H. Tsunemi, S. Kitamoto, K. Hayashida, E. Mitata, K. Hashimotodani, K. Koyama, G. R. Ricker, M. W. Bautz, R. F. Foster, S. E. Kissel, "Calibration of the X-Ray CCD Camera (XIS) for the Astro-E Mission in the Soft Band", *Proc. SPIE*, **3765**, this volume, 1999.
4. P. J. Serlemitsos and Y. Soong, "Foil X-Ray Mirrors", *Astroph. & Sp. Sci.*, **239**, p. 177, 1996.
5. T. Kamae, et al., "Astro-E Hard X-ray Detector", *Proc. SPIE*, **2806**, pp. 314-328, 1996.
6. S. H. Moseley, J. C. Mather, and D. McCammon, "Thermal Detectors as X-ray Spectrometers", *J. Appl. Phys.* **56**, pp. 1257-1262, 1984.
7. C. K. Stahle, M. D. Audley, K. R. Boyce, R. P. Brekosky, R. Fujimoto, K. C. Gendreau, J. D. Gygax, Y. Ishisaki, R. L. Kelley, R. A. McClanahan, T. Mihara, K. Mitsuda, S. H. Moseley, D. B. Mott, F. S. Porter, C. M. Stahle, and A. E. Szymkowiak, "Design and Performance of the Astro-E/XRS Microcalorimeter Array and Anticoincidence Detector" in *Proc. SPIE*, **3765**, this volume, 1999.
8. C. K. Stahle, D. McCammon, and K. D. Irwin, "Quantum Calorimetry", *Physics Today*, Vol. **52**, No. 8, p. 32, August 1999.
9. F. S. Porter, M. J. DiPirro, R. L. Kelley, T. Pham, C. K. Stahle, A. E. Szymkowiak, J. G. Tuttle, M. D. Audley, K. C. Gendreau, R. P. Brekosky, J. D. Gygax, D. McCammon, R. J. Paulos, and S. D. Murphy, "Detector Assembly and the Ultralow-temperature Refrigerator for XRS", *Proc. SPIE*, **3765**, this volume, 1999.
10. D. B. Mott, S. B. Dutta, R. McClanahan, R. P. Brekosky, C. M. Stahle, R. L. Kelley, C. K. Stahle, and A. E. Szymkowiak, "Fabrication of Monolithic Silicon Calorimeters", *Proc. Seventh Int. Workshop on Low Temperature Detectors"*, pp. 119-120, 1997.
11. S. R. Breon, M. J. Dipirro, J. G. Tuttle, P. J. Shirron, B. A. Warner, R. F. Boyle and E. R. Canavan, "Thermal Performance of the XRS Helium Cryostat", to appear in *Advances in Cryogenic Engineering*, **44**, 1999.
12. S. R. Breon, P. Shirron, R. Boyle, E. Canavan, M. DiPirro, A. Serlemitsos, J. Tuttle and P. Whitehouse, "The XRS Low Temperature Cryogenic System: Ground Performance Tests Results", *Cryogenics*, 1999, in press.
13. J. G. Tuttle, T. P. Hait, R. F. Boyle, H. J. Muller, J. D. Hodge, and S. R. Breon, "A High Tc Superconducting Current Lead Assembly for the XDS Helium Cryostat", *Advances in Cryogenic Engineering*, **43**, pp. 965-972, 1998.
14. P. J. Shirron and M. J. DiPirro, "Suppression of Superfluid Film Flow in the XRS Helium Dewar", *Advances in Cryogenic Engineering*, **43**, pp. 949-956, 1998.
15. M.J. DiPirro, P.J. Shirron, and J.G. Tuttle, "Mass gauging and thermometry on the Superfluid Helium On-Orbit Transfer flight demonstration", *Advances in Cryogenic Engineering*, **39**, p. 129, 1994.
16. K. Mitsuda and R. Kelley, "The XRS System - The First Cryogenic X-Ray Detector in Orbit", *NIM*, 1999, in press.
17. F. R. Powell, R. A. M. Keski-Kuha, M. V. Zombeck, R. E. Goddard, G. Chartas, L. K. Townsley, E. Möbius, J. M. Davis and G. M. Mason, *Proc. SPIE*, **3113**, pp. 432-440, 1997.
18. K. R. Boyce, R. G. Baker, J. J. Dumonthier, R. L. Kelley, C. K. Stahle, A. E. Szymkowiak, G. E. Winkert, M. D. Audley, K. C. Gendreau, R. Fujimoto, and Y. Ishisaki, "Design and Performance of the *Astro-E*/XRS Signal Processing System", *Proc. SPIE*, **3765**, this volume, 1999.
19. T. Furusho, N. Y. Yamasaki, Y. Ishisaki, T. Toramatsu, K. Kikuchi, T. Ohashi, K. Mitsuda, and Y. Ogawara, "Filter Wheel System for the X-Ray Microcalorimeter on Board Astro-E", *Proc. SPIE*, **3765**, this volume, 1999.
20. M. D. Audley, K. A. Arnaud, K. C. Gendreau, K. R. Boyce, C. M. Fleetwood, R. L. Kelley, R. A. Keski-Kuha, F. S. Porter, C. K. Stahle, A. E. Szymkowiak, J. L. Tveekrem, R. Fujimoto, K. Mitsuda, Y. Ishisaki, and T. Mihara, "Astro-E/XRS Blocking Filter Calibration", in *Proc. SPIE*, **3765**, this volume, 1999.
21. K. C. Gendreau, M. D. Audley, K. A. Arnaud, K. R. Boyce, R. L. Kelley, F. S. Porter, C. K. Stahle, A. E. Szymkowiak, R. Fujimoto, K. Mitsuda, Y. Ishisaki, and T. Mihara, "*Astro-E*/XRS Calibration Program and Results", *Proc. SPIE*, **3765**, this volume, 1999.